Research Square

Preprints are preliminary reports that have not undergone peer review.
They should not be considered conclusive, used to inform clinical practice,
or referenced by the media as validated information.

Optimizing Rock Fragmentation Uniformity and Kinematic Control in Bench Blasting via the Normalized Decking-Rhodes Parameter (DRP)

Shiqing Zhang
North Blasting Technology Co., Ltd
Zuoming Yin
zuomignyin@163.com

North Blasting Technology Co., Ltd
Zhao Zhang
North Blasting Technology Co., Ltd
Feng Xie
North Blasting Technology Co., Ltd
Chenglei Hao
North Blasting Technology Co., Ltd
Jingjiu Bi
North Blasting Technology Co., Ltd
Liangkui Hua
North Blasting Technology Co., Ltd
Boming Xu
North Blasting Technology Co., Ltd

Article

Keywords: Open-pit uranium mine, Air deck charge configuration, Particle Blast Method (PBM), Decking-Rhodes Parameter(DRP)

Posted Date: February 27th, 2026

DOI: https://doi.org/10.21203/rs.3.rs-8791748/v1

License: This work is licensed under a Creative Commons Attribution 4.0 International License.
Read Full License

Additional Declarations: No competing interests reported.

Article

Optimizing Rock Fragmentation Uniformity and Kinematic Control in Bench Blasting via the Normalized Decking-Rhodes Parameter (DRP)

Shiqing Zhang [1,3],Zuoming Yin [1,2,*], Zhao Zhang [1] , Chenglei Hao [1], Jingjiu Bi [1], Liangkui Hua [1], Boming Xu [1]

[1] North Blasting Technology Co., Ltd, Beijing 100097, China;
[2] Key Laboratory of Ministry of Education for Efficient Mining and Safety of Metal Mines, University of Science and Technology Beijing, Beijing 100083, China;
[3] Beijing institute of technology, Beijing 100081,China
* Correspondence: zuomignyin@163.com;

Abstract

Achieving a balance between effective rock fragmentation and the mitigation of hazardous flyrock (front-row throw effects) is a persistent challenge in open-pit bench blasting. This study investigates the influence of vertically positioned air-deck charges on explosive energy distribution and rock damage evolution. We propose the Decking-Rhodes Parameter (DRP) as a novel, normalized characterization index for air-deck positioning to replace qualitative descriptors. Using a coupled Particle Blast Method (PBM), Finite Element Method (FEM), and Smoothed Particle Hydrodynamics (SPH) numerical framework, complemented by field monitoring at the Husab Uranium Mine, we evaluate the DRP's performance across varying burden conditions. Results indicate that optimal energy utilization and fragmentation uniformity are achieved when the DRP ranges from 0.36 to 0.73. Field applications confirmed that at DRP = 0.73, fragmentation met stringent gradation requirements while significantly reducing excessive top-bench throw.

Keywords: Open-pit uranium mine; Air deck charge configuration; Particle Blast Method (PBM); Decking-Rhodes Parameter（DRP）

1. Introduction

The Husab Uranium Mine, situated in the western desert region of Namibia, is one of the world's largest open-pit operations, utilizing deep-pit mining and advanced road development. With global uranium reserves ranking third, the project involves a massive total excavation volume of 2.1 billion tonnes. The annual production target is approximately 140 million tonnes, primarily focusing on leucogranite-type ore extraction. In this context, high-bench blasting has become essential to accommodate large-scale drilling and loading equipment, reduce stripping costs, and maximize economic returns [1]. Furthermore, optimizing energy partitioning in high-bench blasting is critical for improving fragmentation efficiency and ensuring operational safety.

In conventional bench blasting, only 20%–30% of the explosive energy is effectively utilized for rock fragmentation; the remainder dissipates as parasitic energy in the form of ground vibrations, near-field over-comminution (pulverization), and hazardous flyrock [2]. To mitigate these adverse effects and enhance energy efficiency, researchers have extensively investigated shockwave dynamics within air-decked charge configurations [3]. Engineering practice has confirmed that air-deck structures can regulate the pressure

pulse, optimize fragmentation distribution, and control rock ejection trajectories [4]. However, as bench heights increase to 12–15 m to accommodate larger equipment, maintaining blasting quality while reducing costs remains a significant technical challenge [5–7].

Previous research has explored the mechanisms of air-decked blasting from various perspectives. Kabwe [8] proposed that shockwave oscillations within the air gap enhance the integrity of the surrounding rock, a finding validated by fragment size distribution analysis. Jhanwar and Jethwa [9] demonstrated that air-deck charges significantly reduce both fines and boulders, noting that fragmentation is directly influenced by the air gap length. Fourney et al. [10] observed that in top-air-decked configurations, shockwaves reflected from the stemming can prolong the pressure duration by 2 to 5 times compared to fully coupled charges. This suggests that optimal gap length is achieved when the reflected wave peak pressure exceeds the rock's failure criteria. Further studies by Yang et al. [11] identified optimal directional fracturing at air gap ratios of 33.3%–50%, while Saharan et al. [12] and Roy et al. [13] emphasized the strategic combination of air gaps and stemming to control fumes and enhance energy utilization. Roy et al. [13] successfully applied air deck technology in an Indian underground coal mine, enhancing blasting effects and controlling fumes. Wang Desheng et al. [14-16] established preliminary burden-average fragmentation size relationships through model tests. Li Xianglong et al. [17-21] demonstrated a positive correlation between bench height and throw ratio at Bayan Obo West Mine.

In practice, the nonlinear distribution of the burden along the borehole depth often triggers flyrock hazards [22]. Traditional coupled charges lead to excessive energy absorption in the proximal zone, causing over-pulverization near the borehole [23]. To address this, air gaps are essential for moderating peak pressures [24]. While existing studies confirm the reliability of air-decking for fragmentation, there is a distinct lack of research regarding real-time, stratum-specific rock movement and damage propagation. Furthermore, the absence of unified criteria for air-deck positioning—traditionally described qualitatively—hinders the development of precise detonation product flow models. Chen Shouru et al. [25] studied explosive energy distribution in air deck structures. Ding Chenxi et al. [26] analyzed energy release rates using fractal damage theory. Zuo Jinjing et al. [27] showed inverse proportionality between decoupling coefficient and rock damage. Yang Guoliang et al. [28] investigated directional fracture mechanisms. Zhu Hongbing et al. [29] derived stabilized pressure equations. Wu Liang [30] confirmed inverse correlation between air deck length and comminution zone size. Existing research validates air deck reliability but primarily focuses on post-blast fragmentation morphology, lacking analysis of stratum-specific rock movement and damage propagation. In numerical blast analysis, LS-DYNA addresses detonation-induced nonlinearities. Mitelman et al. [31] combined FEM-DEM to simulate shocks obeying Rankine-Hugoniot relations. In numerical analysis, the integration of the Particle Blast Method (PBM) and Smoothed Particle Hydrodynamics (SPH) has enabled high-fidelity modeling of borehole detonation and gas-solid interactions under extreme conditions [32, 33]. This study addresses the aforementioned gaps by establishing a unified air-deck characterization method. Using a coupled PBM-FEM-SPH framework, we analyze damage patterns and rock velocity profiles across various air-deck positions. These numerical findings are subsequently validated through field monitoring, providing a robust theoretical and empirical foundation for advancing high-bench blasting technology.

2. Characterization of Air Deck Position Parameters

For air deck charge structures, as shown in Figure 1, the air deck length and position are two critical parameters that significantly influence detonation flow. Different charge structures typically employ the air deck ratio parameter (denoting the proportion of air deck length to total charge length) to characterize the configuration:

$$\varphi = \frac{l_a}{l_{e1} + l_a + l_{e2}} \quad (1)$$

where φ is the air deck ratio parameter (air deck length to charge length ratio), l_{e1} is the lower charge length, l_{e2} is the upper charge length, and l_a is the air deck length.

Quantifying air deck position has been challenging, often relying on qualitative terms like "upper," "middle," or "lower." This complicates theoretical calculations for optimal placement. We therefore propose the DRP – a normalized characteristic parameter for air deck position in bench blasting:

$$\mu_j = 1 - \frac{2(h_2 - h_3)}{h_1 - h_3} \quad (2)$$

where μ_j is the Decking-Rhodes Parameter (normalized air deck position), h_1 is the borehole depth, h_2 is the distance from collar to air deck center, and h_3 is the stemming depth.

From Equation (2), for any borehole depth, the air deck position is normalized to $-1 < \mu_j < 1$. When the air deck is located at the borehole bottom, the DRP always falls within $-1 < \mu_j < 0$; when positioned at the top, the DRP remains within $0 < \mu_j < 1$; at $\mu_j = 0$, it corresponds to a central air deck charge where the air deck center coincides with the centroid of the charge segment.

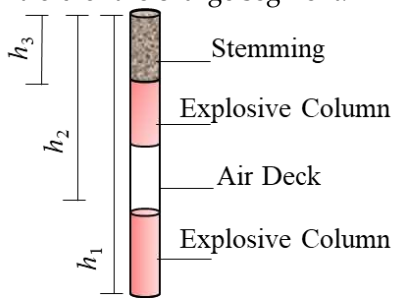


Figure. 1 Schematic of deep-hole air deck charge

Substituting Equation (1) into (2) and expressing with charge length and air deck ratio coefficient yields the transformation:

$$\mu_j = 1 - \frac{l_a + 2l_{e2}}{l_{e1} + l_a + l_{e2}} = 1 - \varphi - \frac{2l_{e2}}{l_{e1} + l_a + l_{e2}} \quad (3)$$

From Equations (1) and (3):

$$\begin{cases} \varphi l_{e1} + \varphi l_{e2} = l_a (1 - \varphi) \\ (\mu_j + 1) l_{e1} + (\mu_j - 1) l_{e2} = \mu_j l_a \end{cases} \quad (4)$$

From Equation (4), the relationship between the lower charge segment l_{e1}, upper charge segment l_{e2}, and air deck length l_a is derived as given by Equation (5):

$$\begin{cases} l_{e1} = \dfrac{(2\varphi - 1)\mu_j l_a}{\varphi} \\ l_{e2} = \left[\dfrac{(\mu_j + 1)(1 - \varphi)}{\varphi} - \mu_j \right] l_a \end{cases} \quad (5)$$

When the air deck is located at the bottom of the charge segment, the charge segment remains entirely in the upper section $l_{e1} = 0$, $l_e = l_{e2}$. Equation (3) then simplifies to:

$$\mu_j = -(1-\varphi) \tag{6}$$

From Equations (3) and (6):

$$\begin{cases} l_{e1} = 0 \\ l_{e2} = l_e = \left(\dfrac{1}{\varphi} - 1\right) l_a \end{cases} \tag{7}$$

When the air deck is located at the top of the charge segment, the charge segment remains entirely in the lower section $l_{e2} = 0,\ l_e = l_{e1}$. Equation (3) then simplifies to:

$$\mu_j = 1 - \varphi \tag{8}$$

From Equations (3) and (8):

$$\begin{cases} l_{e1} = l_e = \left(\dfrac{1}{\varphi} - 1\right) l_a \\ l_{e2} = 0 \end{cases} \tag{9}$$

From Equation (4), when the air deck is at the bottom, always lies within (-1,0). Similarly, from Equation (6), for top air decks, the DRP in (0,1), rigorously validating Equation (0-2). Equation (5) demonstrates that for central air decks, any charge segment length can be expressed solely by the DRP and the air deck ratio parameter. Thus, the combined use of them provides complete and precise quantification of air deck geometry and position. Furthermore, Equations (7) and (9) show that for bottom/top air decks, charge length can be determined by the DRP and the length of air deck alone, rendering the DRP theoretically redundant in such configurations. Alternatively, burden metrics can locate air deck positions (Figure. 2).

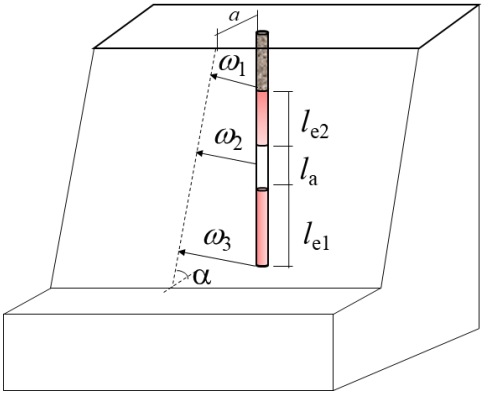


Figure. 2 Burden distribution for different air deck positions

In Figure 2, h_1 defines the borehole depth, h_2 denotes the distance from collar to air deck center, h_3 represents stemming depth, w_1 corresponds to the minimum burden within the charge segment, w_2 indicates burden at air deck center, w_3 signifies maximum burden in the charge segment, a marks crest burden distance, and α is the slope angle.

$$\begin{cases} w_1 = (a\tan\alpha + h_1)cos\alpha \\ w_2 = (a\tan\alpha + h_2)cos\alpha \\ w_3 = (a\tan\alpha + h_3)cos\alpha \end{cases} \tag{10}$$

Based on the design concept of the air-deck charge structure (2), a core parameter is proposed to precisely define the spatial relationship between the charge interval location and the burden.

$$\mu_j = \frac{\frac{1}{2}(w_1 + w_3) - w_2}{\frac{1}{2}(w_1 - w_3)} = 1 - \frac{2(w_2 - w_3)}{w_1 - w_3} \tag{11}$$

Similarly, the normalized parameter for the proposed DRP establishes the foundation for quantitative analysis of deep-hole air-deck charge detonation theory.

3. Calibration and Experimental Validation of Numerical Simulation Parameters

3.1 Calibration of RHT Constitutive Model Parameters for Alaskite

The RHT constitutive model has been widely applied in projectile penetration into concrete and rock blasting simulations with satisfactory results. Among its 38 parameters, seven fundamental parameters can be determined through static mechanical tests: Density, Shear modulus, Uniaxial compressive strength, Uniaxial tensile strength, Initial porosity, Tensile-to-compressive strength ratio, and Shear-to-compressive strength ratio. Table 1 presents the physical and mechanical properties of alaskite obtained from field tests at slope-cut locations

Table 1. Physical-Mechanical Parameters of Alaskite

Rock Type	Density ρ (g/cm^3)	P-wave Velocity V_p (m/s)	Tensile Strength σ_t (MPa)	Compressive Strength σ_c (MPa)	Elastic Modulus E(GPa)	Poisson's Ratio μ	Cohesion C(MPa)	Friction Angle φ (°)
Alaskite	2950	3170	7.84	159.65	24.16	0.238	21.52	53.77

Six parameters govern strain rate effects, with partial parameters predefined by the model. Reference compressive $\dot{\varepsilon}_0^{\mathrm{c}} = 3.0\times10^{-8}\,\mathrm{ms}^{-1}$. Reference tensile strain rates $\dot{\varepsilon}_0^{\mathrm{t}} = 3.0\times10^{-9}\,\mathrm{ms}^{-1}$. Failure compressive $\dot{\varepsilon}^{\mathrm{c}} = 3.0\times10^{22}\,\mathrm{ms}^{-1}$. Failure tensile strain rates $\dot{\varepsilon}^{\mathrm{t}} = 3.0\times10^{22}\,\mathrm{ms}^{-1}$. Strain rate of compressive and tensile exponents calculated as:

$$\beta_c = \frac{4}{20+3f_c}$$
$$\beta_t = \frac{2}{20+f_c} \tag{12}$$

Hugoniot polynomial coefficients are A_1, A_2 and A_3. EOS parameters are B_0, B_1, T_1 and T_2, which satisfy:

$$\begin{gathered} A_1 = \rho_0 c_0^2 \\ A_2 = \rho_0 c_0^2 (2s-1) \\ A_3 = \rho_0 c_0^2 \left(3s^2 - 4s + 1\right) \\ T_1 = \rho_0 c_0^2 \\ B_0 = B_1 = 2s-1 \\ T_2 = 0 \end{gathered} \tag{13}$$

Where A_1, A_2 and A_3 are the Hugoniot polynomial coefficients. c_0 denotes the bulk sound speed of the material at zero pressure. *S* is an empirical coefficient with lithology-dependent values as provided in Meyers' seminal work (Meyers, 1994): Marble: s = 0.95; Granite: s = 1.2. The damage parameters D1 and D2 are initially set to 0.04 and 1 respectively. The minimum residual strain at failure $\varepsilon_p^{\mathrm{m}}$ is related to damage and is taken as 0.01. The strength-related parameter P_{crush} represents the elastic limit pressure of the material, which can be obtained from $P_{\mathrm{crush}} = 2f_c/3$. The tensile-compressive meridian ratio parameter Q and the Lode angle correlation coefficient B can be fitted to obtain Q = 0.68 and B = 0.05. The failure surface parameters A and N can be obtained from the failure surface expression when $3P_0^* \geqslant F_{\mathrm{r}}$. When the material is under quasi-static loading conditions, F_r is taken as 1. Therefore, when $3P_0^* \geqslant F_{\mathrm{r}}$, the definition formula of the failure surface curve is as follows:

$$\sigma_f^*\left(P_0^*,F_r\right)=\begin{cases} A\left(P_0^*-F_r/3+\left(A/F_r\right)^{-1/N}\right)^N & 3P_0^*\geq F_r \\ F_rF_s^*/Q_1+3P_0^*\left(1-F_s^*/Q_1\right) & F_r>3P_0^*\geq 0 \\ F_rF_s^*/Q_1-3P_0^*\left(1/Q_2-F_s^*/\left(F_t^*Q_1\right)\right) & 0>3P_0^*\geq 3P_t^* \\ 0 & 3P_t^*>3P_0^* \end{cases} \quad (14)$$

$$\sigma_{\mathrm{f}}^*=A\left(P_0^*-1/3+(A)^{-1/N}\right)^N \quad (15)$$

$$P_0^*=\left(\sigma_1+2\sigma_3\right)/3f_{\mathrm{c}} \quad (16)$$

$$\sigma_{\mathrm{f}}^*=\sigma_1-\sigma_3/f_{\mathrm{c}} \quad (17)$$

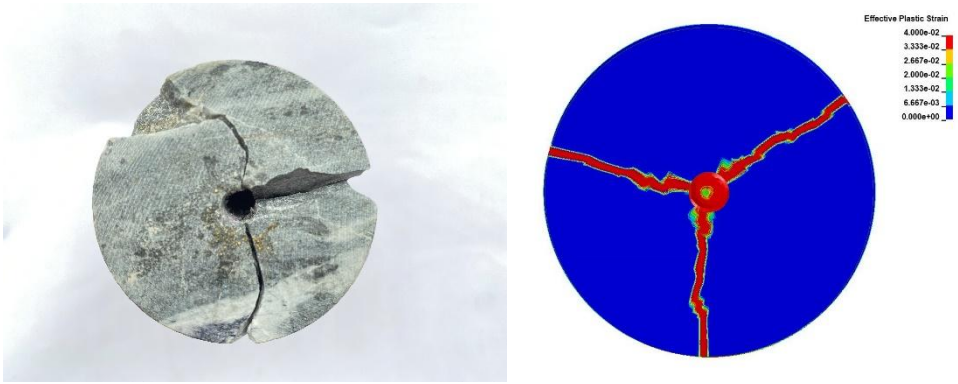
The triaxial confining pressure relationship is estimated from the uniaxial compressive strength based on the Hoek-Brown strength criterion. The pore pressure at compaction P_{comp} is 6 GPa. The porosity index n_p is 3. The shear modulus reduction coefficient ξ is 0.5. The remaining four parameters are determined through debugging and set as follows: the compression yield surface parameter g_c^* is 0.53, the tension yield surface parameter g_t^* is 0.7, the residual stress strength parameter A_f is 1.6, and the residual stress strength index n_f is 0.61. Some scholars have determined the order of influence of each factor through range analysis, obtaining that the compression yield surface parameter g_c^* has the greatest impact on the numerical simulation results, while the minimum effective strain $\varepsilon_p^{\mathrm{m}}$ has the least impact. System parameters: the unit system parameter onempa is set to 0; Gruneisen gamma is set to 0; the erosion plastic strain is set to 2.0.

3.2 Experimental Validation of RHT Constitutive Model Parameters

Experimental specimens with dimensions of diameter D = 50 mm and height H = 100 mm were prepared. A borehole of diameter φ = 3 mm and depth L = 70 mm was drilled axially. The charge consisted of lead azide (150 mg) packed in a thin plastic tube (2 mm diameter, 50 mm charge height), sealed at both ends with modeling clay (20 mm plug length). Detonation was initiated by high-voltage electric discharge via a 0.5 mm enamel-coated wire positioned at the borehole base. The borehole was stemmed with sand particles bonded by cyanoacrylate adhesive. Post-blast failure patterns exhibited close agreement with numerical simulations.



(a) Post-blast specimen; (b) 3D simulation;



(c) Top view of fractures; (d) Simulated fracture network (top view).

Figure 3. Experimental and numerical comparison of alaskite blasting

The experimental model employed a bottom-hole initiation configuration. Following explosive initiation, the detonation wave propagated spherically outward from the origin. The shock wave advanced unidirectionally upward along the borehole axis. A portion of the shock waves, influenced by flow deflection angles, intersected near the initiation point. This interaction resulted in the formation of a localized high-pressure zone with pressures exceeding the detonation pressure, leading to significant damage, as illustrated in Figure 3(a).

As detonation propagated upwards, the upper explosive charge experienced dual-directional flow dynamics during shock wave expansion. Consequently, X-shaped shock wave intersections formed both ahead of and behind the reaction zone due to the effects of shock wave flow deflection angles.

Upon completion of detonation propagation, the shock wave reached the air deck section. With no further energy supplied by explosive reaction, the continuous explosive column and the air deck collectively formed a structure analogous to a Laval nozzle. The extremely high pressure within this air deck section generated a damage zone significantly larger than that observed within the explosive column itself.

Subsequent shock wave reflection and transmission occurred at the interface between the air deck and the stemming material. Due to the high porosity of the loose stemming, a significant portion of the shock wave energy was consumed in performing compressive work on the stemming material. Simultaneously, shock waves propagating in the direction opposite to the detonation front (originating from the detonation tail) and partially reflected shock waves from the stemming interface converged. This convergence formed a secondary high-pressure zone.

However, energy dissipation through compressive work on the stemming material resulted in a lower peak pressure within this secondary high-pressure zone compared to the peak pressure observed at the bottom of the borehole.

4. Establishment of Numerical Model

4.1 Development of PBM-FEM-SPH Coupled Model

For deep-hole bench blasting, the insufficient fragmentation in the stemming zone under reduced top burden conditions constitutes the primary factor necessitating increased air-deck length. Air-decks of identical proportional lengths at different positions exert distinct influences on the borehole periphery. The central air-deck configuration yields, minimum fractal dimension across cross-sections, higher coefficient of variation compared to full-column charges, and lower coefficient of variation than top air-deck charges.

This charge structure generates fewer fractures and reduced damage in rock media while maintaining balanced damage distribution across profiles. Critically, blast-induced

cracks propagating through the air-deck segment do not undergo abrupt reduction due to pressure decay. Consequently, numerical simulations investigated five DSP values (0.73, 0.36, 0, -0.36, -0.73) for vertical boreholes with a fixed decking ratio of 0.27. The corresponding charge structures are illustrated in Figure 4.

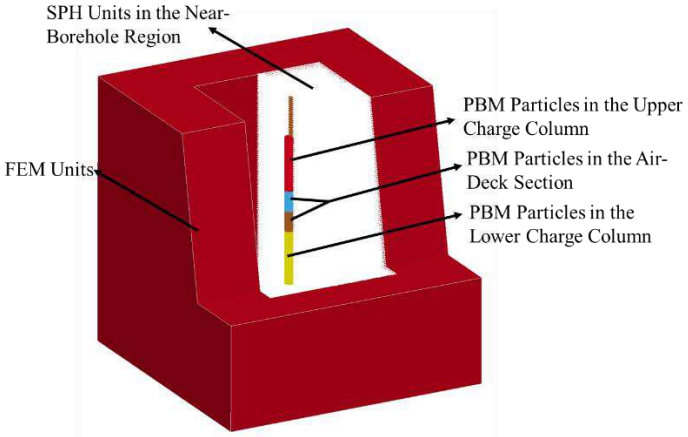
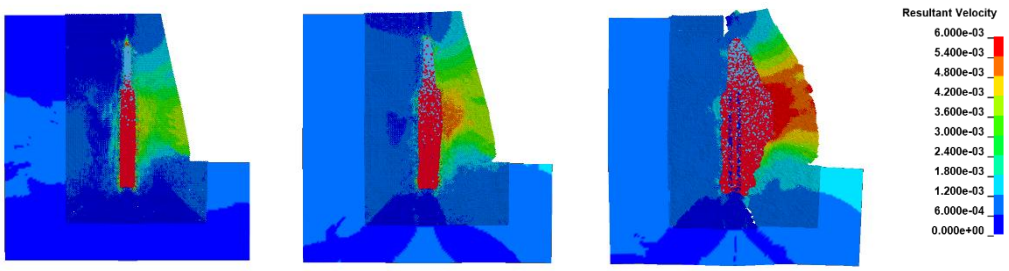


Figure 4. Schematic diagram of the numerical simulation model for the DSP

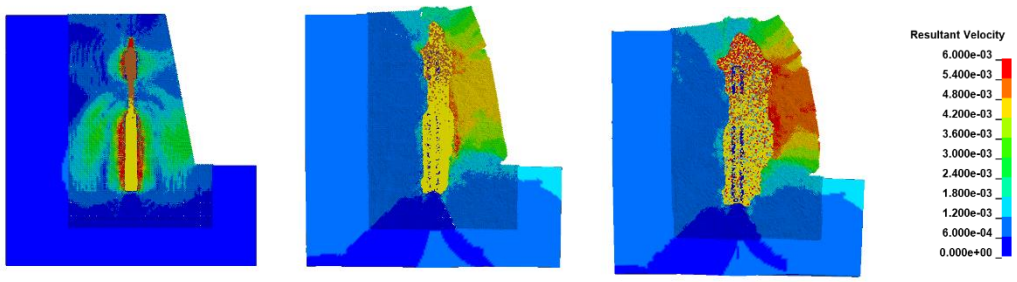
4.2 Analysis of Velocity Variation on Slope Surface for Different Air-Deck Positions

SPH particles are controlled through kernel functions. When displacement deformation becomes extremely large, calculations fail to converge and errors accumulate continuously. When simulating rock mass damage, the damage magnitude keeps expanding under such conditions. As the original kernel functions become invalid under excessive deformation or displacement, only results within three times the detonation duration were selected for statistical analysis of rock mass damage effects. As the air-deck position lowers, the burden corresponding to the air-deck section gradually increases. Simultaneously, the charge structure transitions to a central air-deck configuration. Using reverse initiation, pressure in the upper charge segment rapidly decreases due to rarefaction waves reflected from the air-deck section. Meanwhile, detonation wave flow from the lower charge segment significantly increases quasi-static pressure in the upper section. With simultaneous initiation of upper and lower charges, upper detonation wave drive compressed air downward. Detonation wave from upper and lower segments converge to form an interaction zone. Detonation wave from the lower segment reflect at the top stemming zone and flow downward. Under the combined action of upper and lower detonation wave, stemming material ejects upward, causing rapid pressure reduction in the borehole. After reflection dynamics, detonation wave reflected from the top reach the hole bottom but cause negligible pressure increase in the lower borehole. This results from pressure reduction caused by ejected stemming material in the upper section and the high mass density of detonation wave. Following massive upward outflow of detonation wave, borehole pressure approaches atmospheric levels.



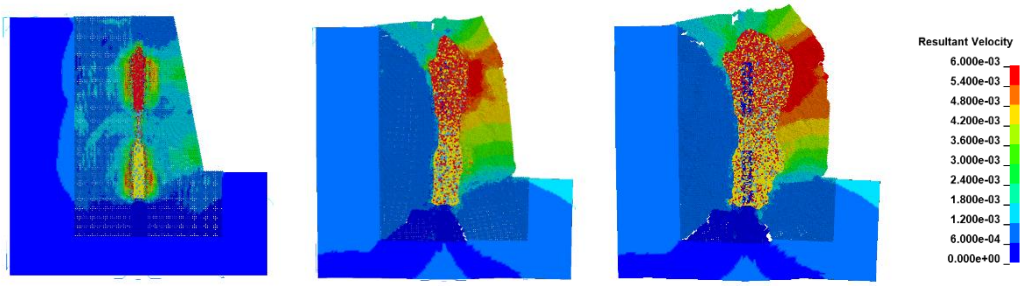
(a) Completion of explosive detonation (b) Detonation wave to top (c) Slope surface bulge formation

Figure 5. Velocity contour at cross-section for DRP μ_j=0.73



(a) Completion of explosive detonation(b) Detonation wave to top(c) Slope surface bulge formation

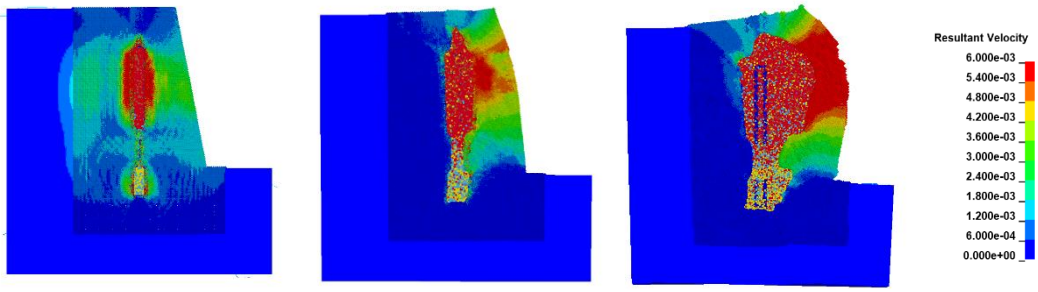
Figure 6. Velocity contour at cross-section for DRP μ_j=0.36



(a) Completion of explosive detonation(b) Detonation wave to top(c) Slope surface bulge formation

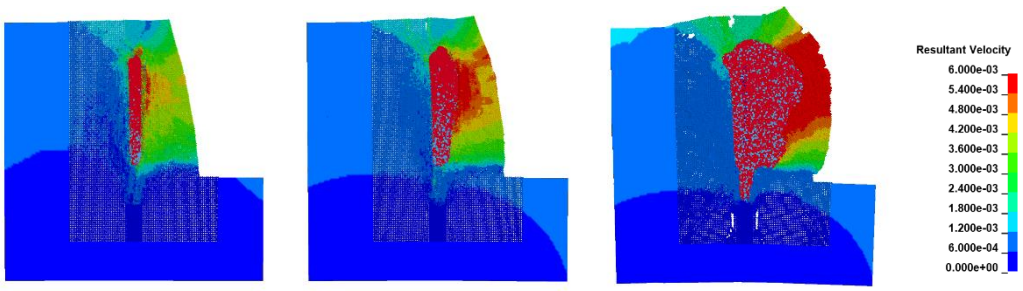
Figure 7. Velocity contour at cross-section for DRP μ_j=0

As shown in Figure 5, when μ_j=0.73 , the maximum free-face velocity (average ≈46 m/s) occurs at the charge/air-deck interface. For μ_j=0.36 (Figure 6), combined upper/lower charge interaction with reverse initiation in the upper segment causes significant pressure reduction. The lower charge transfers more energy to rock fragmentation due to burden effects, resulting in markedly decreased slope surface velocity. For μ_j=0 (Figure 7), symmetric charge lengths with reverse initiation in the upper segment exhibit reduced pressure. However, the smaller burden in the upper section generates higher rock movement velocity (peak 58 m/s) at the slope surface.



(a) Completion of explosive detonation(b) Detonation wave to top(c) Slope surface bulge formation

Figure 8. Velocity contour at cross-section for DRP μ_j=-0.36



(a) Completion of explosive detonation(b) Detonation wave to top(c) Slope surface bulge formation

Figure 9. Velocity contour at cross-section for DRP μ_j=-0.73

As shown in Figs. 8 and 9, when the DRP μ_j takes values of -0.36 and -0.73, the maximum free-face velocity (62 m/s) occurs near the upper charge segment where burden is minimal. Significant ejection effects are observed. Meanwhile, at the high-burden bench base beneath the air-deck, reduced borehole pressure results in insufficient fragmentation energy. The upper section with minimal burden experiences rapid fracture propagation, directing substantial blast gases toward rock ejection. Consequently, this leads to toe formation ranging from 0.5 to 1.6 meters in the high-burden lower region. Optimal decking parameters correlate directly with local burden magnitude: Larger burden corresponds to smaller μ_j and larger burden corresponds to smaller decking ratio.

Under identical blast parameters, rock properties influence decking ratio selection. Comparative analysis of slope velocities across air-deck positions (Figure 10) demonstrates μ_j's directional influence on energy evolution during blasting. For bench blasting: Smaller burdens require larger μ_j values, and reduced fragmentation energy is needed. Vertical borehole blasting exhibits smaller top burdens and larger base burdens. Therefore, μ_j values within the (0.36, 0.73) range effectively maximize explosive energy utilization.

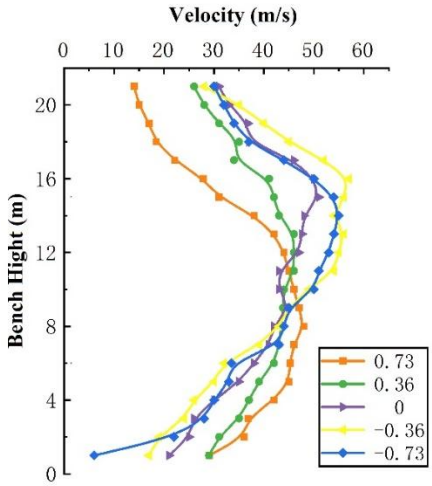


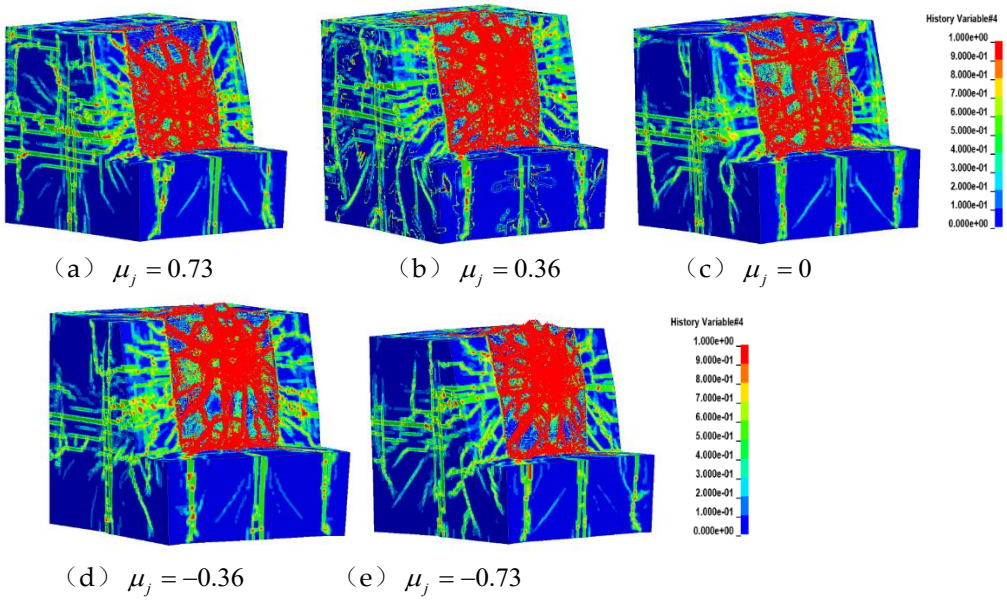
Figure 10. Slope surface velocity profiles for different air-deck positions

Comparative analysis reveals that the DRP should fall within the (0.36, 0.73) range, while the peak specific impulse on the borehole wall remains concentrated at the hole bottom. Simulation results demonstrate that in vertical borehole air-deck blasting, the crushing zone near the borehole (caused by abrupt detonation pressure) is significantly reduced. The radial and axial fracture propagation zones are substantially expanded, thereby effectively improving explosive energy utilization efficiency.

4.3 Analysis of Fragmentation Effects for Different Air-Deck Positions

The final free-surface morphologies corresponding to various air-deck positions are presented in Figure 11. In deep-hole bench blasting with air-deck charges, the cavity position significantly influences the flow dynamics of detonation wave within the borehole after explosive detonation, thereby altering the mechanism of explosive energy transfer to the near-field rock mass. Explosive energy acts on the proximal rock mass through multiple pulsed loadings rather than instantaneously as occurs in concentrated charge blasting. The air-deck functions as a regulatory mechanism by initially storing energy and subsequently releasing it in discrete pulses.

The explosive performance of air-deck charges fundamentally originates from the expansion of gaseous wave coupled with multiple interactions: shock waves within the air column, shock waves interacting with the stemming zone, and shock waves impacting the hole bottom. This phenomenon generates secondary shock waves that repeatedly load the near-field rock mass over extended durations. For the DRP (upper air-deck) and μ_j=-0.73 (bottom air-deck), the bottom air-deck configuration exhibits extensive unfragmented zones at the bench base due to constraints imposed by the large burden, as illustrated in Figure 11(e).



（a） $\mu_j = 0.73$ （b） $\mu_j = 0.36$ （c） $\mu_j = 0$

（d） $\mu_j = -0.36$ （e） $\mu_j = -0.73$

Figure 11. Three-dimensional numerical simulation diagrams of air-deck charges at different positions

As shown in Figure 12, comparative analysis of cross-sectional damage patterns across different air-deck positions reveals progressively intensified rock fragmentation in the minimally burdened upper sections as the DRP decreases. Integrating observations from Figure 10, explosive detonation drives excessive rock ejection from slope surfaces, resulting in significant energy dissipation. Larger η values correspond to lower velocities at slope monitoring points. Consequently, for vertical borehole air-deck blasting in open-pit benches, the DRP should be maintained within the 0.36 to 0.73 range, with air-decks positioned in the upper-middle segment of the charge column. Central air-deck configurations (η=0) are unsuitable for practical implementation.

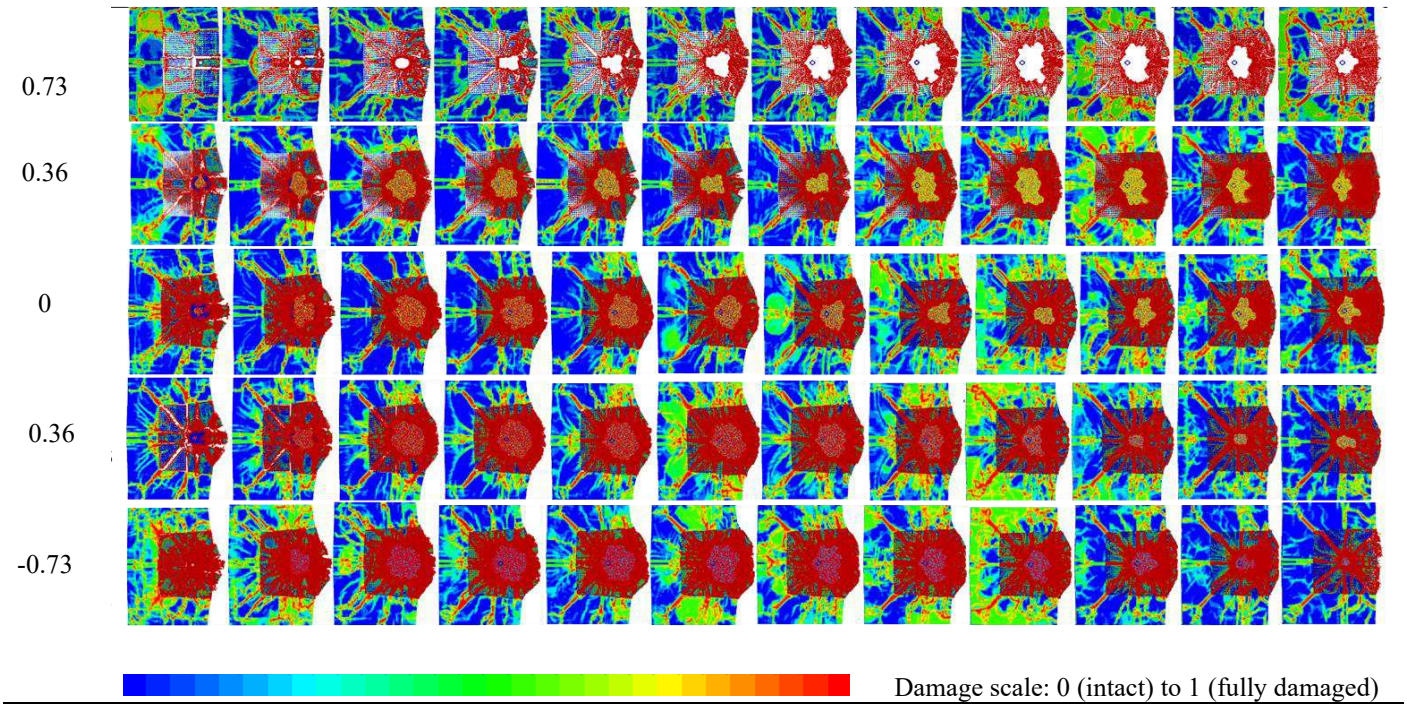


Figure 12. Cross-sectional damage diagrams for different air-deck positions

5. Field Application

The blasting process with air-deck charges in open-pit benches involves extreme complexity, as detonation dynamics and gas flow within boreholes are unobservable. Quantifying air-deck effects on borehole pressure proves particularly challenging during large-scale operations. Field application were conducted at the Husab Uranium Mine in Namibia (Figure 13), using explosive materials detailed in Table 2.

Table 2. Blasting Material Parameters

Material	Specification/Parameters	Manufacturer	Remarks
ANFO	Granularity: >95% (2.5-3.0 mm); Density: 0.83 g/cm³; Detonation velocity: 3800-4200 m/s	AEL	
Detonator	400 g	AEL	
Downhole tube	18 m × 500 ms	AEL	
Surface tube	9 m × 0 ms	AEL	
Air-deck bag	58 cm × 113 cm circumference; 50 cm × 63 cm circumference	AEL	Inflated height: 40 cm; Diameter: 34 cm/17 cm

Blasting results demonstrate negligible differences in rock fragmentation across air-deck configurations. However, forward throw distance exhibits an increasing trend as decking length decreases. Fragmentation analysis software was employed to quantify size distributions of rock from different decking-length zones, with results presented in Figure 14 and Table 3.



Figure 13. Field test site

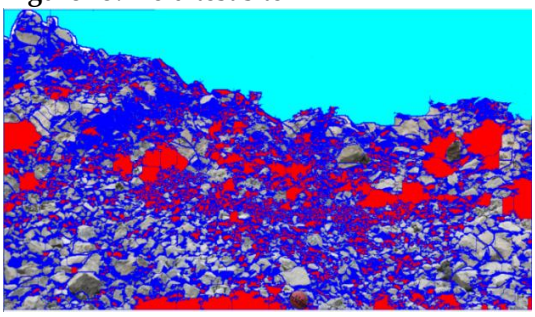


Figure 14. Fragmentation size distribution analysis

As evidenced in Table 3, fragmentation gradation is co-influenced by borehole diameter and decking length. To enhance loading efficiency, Husab Mine mandates specific fragmentation standards for non-ore zones: 100% of fragments ≤1200 mm, 90% of fragments ≤600 mm, and 80% of fragments ≤400 mm. For 311 mm boreholes at μ_j=0.73 : 2.5 m decking: Zero oversize fragments (>1200 mm), fully compliant with gradation requirements. 3.0 m decking: Highest oversize fragment percentage. A positive correlation exists between optimal decking length and borehole diameter.

Table 3. Post-blast fragmentation distribution

Borehole diameter (mm)	Decking length (m)	≤1200 mm (%)	≤1000 mm (%)	≤600 mm (%)	≤500 mm (%)	≤400 mm (%)
311	2.0	94.12	92.11	87.20	82.11	77.02
	2.5	100.00	95.07	90.46	83.61	81.58
	3.0	91.22	90.02	83.51		

6. Conclusions

This study establishes a systematic framework for optimizing air-deck positioning in vertical bench blasting to maximize explosive energy utilization. By integrating the novel Decking-Rhodes Parameter (DRP) with high-fidelity numerical modeling and field validation, the following conclusions are drawn:

(1) Standardization of the Decking-Rhodes Parameter (DRP): The newly proposed Decking-Rhodes Parameter (μ_j) provides a robust, standardized metric for quantifying the spatial positioning of air cavities within a borehole. Unlike qualitative descriptors, the DRP allows for a precise mathematical correlation between air-deck placement and burden magnitude. The parameter effectively directs the spatial evolution of detonation energy, ensuring that energy density is partitioned according to the varying resistance of the rock mass along the bench face.

(2) Optimal DRP for Linearly Varying Burdens: In bench blasting scenarios characterized by non-uniform burdens (minimal at the crest and maximal at the toe), DRP values ranging from **0.36 to 0.73** were found to maximize energy efficiency. The investigation

demonstrates that central air-deck configurations (μ_j=0) are mechanically suboptimal for vertical holes; instead, the reduced resistance of the upper burden necessitates higher positive DRP values (top-decking) to moderate the fragmentation energy and prevent excessive rock throw.

(3) Field Validation and Scale Effects: Field verification at the Husab Uranium Mine using 311 mm diameter boreholes confirmed the predictive accuracy of the DRP model. At a DRP of **0.73**, a 2.5 m air-deck successfully eliminated oversized fragments (>1200 mm) and met all required gradation specifications. Conversely, increasing the decking length to 3.0 m led to insufficient energy density, resulting in a significant increase in the boulder percentage. These results indicate a distinct positive correlation between the optimal air-deck length and borehole diameter, suggesting that larger diameters allow for more expansive air-decking without compromising fragmentation quality.

Acknowledgement： All data generated or analysed during this study are included in this published article.

Funding: This research was funded the Key Laboratory of Ministry of Education of China for Efficient Mining and Safety of Metal Mines（No.ustbmslab202403）

References

1. Melnikov. Charge construction influence on explosion operations efficiency[R]. Reports of the YI science symposium on drilling, explosives, explosion operations and study of physical and mechanical properties of rocks, (Rolla, USA), Gosgortekhizdat (1962).
2. Melnikov,Marchenkov. Effective methods of application of explosion[C]. 12th U.S. Symposium on Rock Mechanics (New York, AIME), Chap. 18, (1971): 359-378.
3. Pal Roy P , Singh R B , Mondal S K. Air-deck Blasting in Opencast Mines Using Low Cost Wooden Spacers for Efficient Utilisation of Explosive Energy[J]. Journal of Mines, Metals & Fuels, 1995 ,43 (8) : 5-15.
4. Moxon N. T. ,Mead D. , Richardson S. B. Air-decked blasting techniques: Some collaborative experiments[J]. Transactions of the Institution of Mining & Metallurgy, Section A: Mining Industry , v102 Jan-Apr 1993: A25-A30.
5. ZHU Hong-bing. Study on the mechanism and application of air-decking blasting［D］. Wuhan: Wuhan University, 2006.
6. CHEN Hui, SHI Xiu-zhi, GUAN Wei-ming. Experimental study on blasting charge structure of layered rock mass ［J］. Journal of Xinjiang University(Natural Science Edition), 2019, 36(3) :361-368.
7. JIA Y Q, GU C L, SHI W Q. The method and application of overcoming the resistance line through high step blasting in open-pit mines [J]. China Mining, 2020, 29 (08): 138-142
8. Kabwe, Eugie. Improving Collar Zone Fragmentation by Top Air-Deck Blasting Technique[J]. Geotechnical and Geological Engineering, 2017,35(1):157-167.
9. J., C., Jhanwar J., et al. The use of air decks in pRhodesuction blasting in an open pit coal mine[J]. Geotechnical & Geological Engineering, 2000.
10. Fourney W L, Barker D B, Holloway D C. Model studies of explosive well stimulation techniques[J]. International Journal of Rock Mechanics and Mining Science & Geomechanics Abstracts, 1981,18(2):113-127.
11. Yang G L, Yang R S, Huo C, et al. Numerical Simulation of Air-Deck Slotted Charge Blasting[J]. Advanced Materials Research, 2011,143-144:787-791.
12. Saharan M R, Sazid M, Singh T N. Explosive Energy Utilization Enhancement with Air-Decking and Stemming Plug, 'SPARSH'[J]. Procedia Engineering, 2017,191:1211-1217.
13. Roy S K, Singh R R, Kumar R, et al. Studies into possible use of air decking in solid blasting in Indian underground coal mines[J]. Mining Technology, 2008,117(2):83-92.
14. ZHOU N , WANG D S, WANG H , etc. Numerical analysis of high step blasting in open-pit mines [J]. Geotechnical Mechanics, 2013, 34 (S1): 516-522+532
15. DUAN J, WU L, ZHANG P F. Research and Application of the Optimal Chassis Resistance Line for High Step Blasting in Barun Mine [J]. China Mining, 2020, 29 (S1): 465-469
16. WANG D S. Research on the fragmentation characteristics of high platform blasting [J]. Nonferrous Metals (Mining Part), 2000, (01): 29-32

17. LIU Z Q, WANG D S, CUI F, etc. Experimental Study on 24m High Step Blasting Technology in Barun Mine [J]. Metal Mines, 2019, (06): 68-71
18. LI X L, HE L H, LUAN L F, etc. Simulation of the shape of the blasting pile caused by high step throwing and blasting in open-pit coal mines [J]. Coal Journal, 2011, 36 (09): 1457-1462
19. LI X L, LIU D S, HE L H, etc. The influence of step height on throwing rate in open-pit coal mines [J]. Explosion and Impact, 2012, 32 (02): 211-215
20. HUANG Y H, LIU D S, LI S L, etc. Numerical simulation of velocity law of high platform throwing blasting [J]. Explosion and Impact, 2014, 34 (04): 495-500
21. LI X L, HE L H. Classification Weibull Model for Predicting the Form of High Platform Throwing Blasting Pile [J]. Explosion and Impact, 2013, 33 (S1): 122-129
22. JIN X , GAO J M, SU H W, etc Experimental study on interval charge blasting of deep hole bench blasting in open-pit mines [J]. Blasting, 2023, 40 (02): 42-47
23. GAO J ,ZHANG L .Evolutionary game analysis of behavioral strategies between government agencies and coal companies -- air interval charge blasting technology promotion[J].Energy,2025,314134236-134236.
24. LI Q ,WEI X ,LI X , et al.Measurement and Stress Response Analysis of Complete History of Blast-Induced Wall Pressure for Boreholes: A Case with Air-Deck Charge[J].Rock Mechanics and Rock Engineering,2024,57(11):9429-9443.
25. Chen S R, Xing D S, Song G M, etc. Comprehensive measures for reducing the large block rate of hard rock step deep hole blasting [J]. Nonferrous Metals (Mining Part), 2002, (02): 34-36
26. CHENXI D ,RENSHU Y ,ZHEN L , et al.Fractal damage and crack propagation in decoupled charge blasting[J].Soil Dynamics and Earthquake Engineering,2020,(prepublish):106503-.
27. JINJING Z ,RENSHU Y ,MIN G , et al.Fracture characteristics of iron ore under uncoupled blast loading[J].International Journal of Mining Science and Technology,2022,32(4):657-667.
28. YANG G L, CHENG S J, WANG P, etc. Axial uncoupled explosive blasting experiment of slotted tube [J]. Explosion and Impact, 2017, 37 (01): 134-139
29. ZHU H B, LU W B, WU L. Research on the Mechanism of Air Interval Charging Blasting [J]. Geotechnical Mechanics, 2007, (05): 986-990
30. WU L, ZHONG D W, CAI L J. Numerical analysis of smooth blasting mechanism in air gap charges [J]. Journal of Wuhan University of Technology, 2009,31 (16): 77-81+149
31. MITELMAN A ,ELMO D .Modelling of blast-induced damage in tunnels using a hybrid finite-discrete numerical approach[J].Journal of Rock Mechanics and Geotechnical Engineering,2014,6(06):565-573.
32. SHAHRIN I M ,ABDULLAH A R ,JEON S , et al.Numerical simulation of rock fragmentation by blasting using Discrete Element Method and Particle Blast Method[J].IOP Conference Series: Materials Science and Engineering,2019,527(1):012032 (8pp).
33. FAKHIMI A ,LANARI M .DEM–SPH simulation of rock blasting[J].Computers and Geotechnics,2014,55158-164.